

Practical Considerations for Measuring Global Spin Density Matrix Elements of Vector Mesons in Heavy-Ion Collisions

Gavin Wilks,¹ Xu Sun,^{2,3,4} and Zhenyu Ye⁵

¹*University of Illinois at Chicago, Chicago, Illinois 60607, USA*

²*The Institute of Modern Physics, Chinese Academy of Sciences, Lanzhou 730000, China*

³*School of Nuclear Science and Technology, University of Chinese Academy of Sciences, Beijing 100049, China*

⁴*State Key Laboratory of Heavy Ion Science and Technology,*

Institute of Modern Physics, Chinese Academy of Sciences, Lanzhou 730000, China

⁵*Lawrence Berkeley National Laboratory, Berkeley, CA 94720*

(Dated: October 23, 2025)

The STAR Collaboration has reported a significant ϕ -meson global spin alignment (ρ_{00}) signal in Au+Au collisions at $\sqrt{s_{NN}} \leq 62$ GeV by measuring the polar angle distribution of ϕ -meson daughters with respect to the orbital angular momentum (OAM) direction of the collision system. In this paper, a new method is explored for studying vector-meson global spin alignment in heavy-ion collisions by examining the two dimensional polar and azimuthal angle distribution. This method allows simultaneous extraction of ρ_{00} and off-diagonal spin density matrix elements (SDMEs), providing unique access to local quark-antiquark spin correlations and spin hydrodynamics in quark-gluon plasma (QGP). The new 2D method also removes potential biases from non-zero off-diagonal SDMEs on ρ_{00} with the 1D method. A detailed procedure to correct for detector acceptance and resolution effects is also presented and validated by simulation studies.

I. INTRODUCTION

Since the discovery of a positive ϕ -meson global spin alignment ($\rho_{00} > 1/3$) in Au+Au collisions at $\sqrt{s_{NN}} \leq 62$ GeV [1, 2], significant effort has been put towards understanding the origin of the signal. It is challenging by conventional mechanisms [3–7] to simultaneously describe the observed ϕ -meson ρ_{00} and the global spin polarization P_H of Λ baryons [8–11]. Several new models have been proposed to accommodate these signals seen by the STAR Collaboration. One model postulates the existence of a ϕ -meson strong force field, where fluctuations in this field would induce global spin alignment [12–16]. Another model, which utilizes gauge/gravity duality, suggests that a non-zero helicity-frame spin alignment induced by the motion of $s\bar{s}$ pairs relative to the thermal background in heavy-ion collisions can generate a global spin alignment signal compatible with the data [17]. A more recent model introduces local strange-quark-antiquark spin correlations to describe the ϕ -meson ρ_{00} and Λ -baryon P_H signals [18]. This model also predicts nonzero off-diagonal spin density matrix elements (SDMEs). Therefore, it is very interesting to experimentally measure the off-diagonal SDMEs and compare them with the model predictions.

The ϕ -meson ρ_{00} results from the STAR Collaboration utilized a 1-dimensional (1D) approach, where only the polar angular (θ^*) dimension was considered [1, 2]. When integrating over the azimuthal angle β , it was assumed that the off-diagonal SDMEs are zero. Biases from off-diagonal SDMEs to extracted ρ_{00} in the presence of event plane smearing have been discussed in Ref. [19].

In addition to the possible impact of off-diagonal SDMEs on the extraction of ρ_{00} , these elements can influence observables of the chiral magnetic effect (CME). Specifically, the spin coherence parameter $\text{Re}(\rho_{1-1})$ for

the ρ meson has been shown to have an effect on the CME observables related to the $\Delta\gamma_{112}$ correlator, the R_{Ψ_2} (ΔS) correlator, and the signed balance functions [20]. Off-diagonal SDMEs can also directly probe how different components of the angular momentum project onto spin space; therefore, making them crucial for understanding hadronization in vortical environments [21–23].

In this paper, a method is introduced to simultaneously extract ρ_{00} and off-diagonal SDMEs by studying both polar and azimuthal angular dimensions, eliminating potential biases from off-diagonal SDMEs to ρ_{00} . The event plane resolution corrections are analytically solved for all SDME quantities and Monte Carlo simulations are used to confirm the formalism, highlighting the importance of considering event plane smearing in efficiency corrections. The effect of the transverse momentum (p_T) resolution is also considered, which could bias ρ_{00} and off-diagonal SDMEs when not considered properly in the correction procedure. A detailed procedure to correct for detector acceptance and resolution effects is also presented and validated by simulation studies.

II. GLOBAL SPIN DENSITY MATRIX ELEMENTS OF VECTOR MESONS

For spin-1 vector mesons, the probability densities of spin states are captured by the 3×3 spin density matrix, ρ . The ρ matrix is a Hermitian positive semi-definite matrix with unit trace. The global spin alignment signal is quantified by the diagonal element ρ_{00} , which indicates the probability density of vector mesons in the spin-0 state. A deviation of ρ_{00} from 1/3, indicates a global spin alignment signal. The off diagonal elements $\rho_{mm'}$ ($m \neq m'$), indicate the quantum coherence between the 3 spin states. Considering a two-body decay of a vector

meson into two pseudo-scalar mesons, the 2-dimensional angular distribution of a daughter in the vector meson's rest frame is:

$$\frac{d^2N}{d\cos\theta^*d\beta} = \frac{3}{8\pi} \left[(1 - \rho_{00}) + (3\rho_{00} - 1) \cos^2\theta^* \right. \\ \left. - \sqrt{2}\text{Re}(\rho_{10} - \rho_{0-1}) \sin 2\theta^* \cos \beta \right. \\ \left. + \sqrt{2}\text{Im}(\rho_{10} - \rho_{0-1}) \sin 2\theta^* \sin \beta \right. \\ \left. - 2\text{Re}(\rho_{1-1}) \sin^2\theta^* \cos 2\beta \right. \\ \left. + 2\text{Im}(\rho_{1-1}) \sin^2\theta^* \sin 2\beta \right], \quad (1)$$

where θ^* is the polar angle between the quantization axis (global frame $+z$ -axis, OAM direction) and the daughter's momentum vector, and β is the azimuthal angle of the daughter's momentum vector in the reaction plane relative to the beam direction (global frame $+x$ -axis) [7, 24]. Figure 1 depicts the θ^* and β angles in the global frame. In the global frame, the $+x$ -axis is along the beam direction, the $+y$ -axis is antiparallel to the impact parameter (\hat{b}), and $+z$ -axis completes the right-hand coordinate system and is aligned with the orbital angular momentum (OAM) direction. This is different than the lab frame, where the $+z$ -axis is along the beam direction, the $+y$ -axis is orthogonal to the ground, while the $+x$ -axis completes the right hand coordinate system. The azimuthal angle of the reaction plane in the lab frame is known as the angle of the reaction plane, Ψ_r , where the reaction plane spans the beam direction and \hat{b} .

Due to a finite number of particles produced in heavy-ion collisions and a finite detector acceptance, the true angle Ψ_r of \hat{b} cannot be known. Therefore, approximation methods described in [25] are used to estimate Ψ_r . The particle emission angle relative to the reaction plane can be written as a Fourier series:

$$\frac{dN}{d\phi} = \frac{1}{2\pi} \left(1 + \sum_{m=1}^{\infty} 2v_m \cos[m(\phi - \Psi_m)] \right). \quad (2)$$

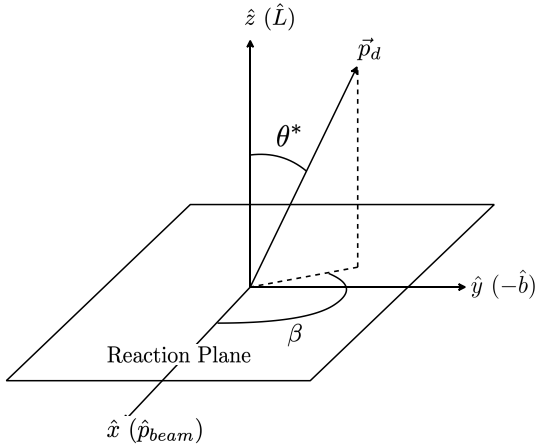


FIG. 1. Global frame coordinate system: \vec{p}_d is the momentum of a daughter particle in the vector meson's rest frame.

Through this decomposition, the angle of the reaction plane can be estimated for each harmonic order, m , known as the event plane angle, Ψ_m [26].

When estimating the reaction plane using harmonic event planes, there is an associated resolution, calculated by,

$$R_m = \langle \cos[m(\Psi_m - \Psi_r)] \rangle, \quad (3)$$

where $\langle \rangle$ represents the average over many events. Throughout this paper, the following definition is used:

$$\Delta\Psi_m = \Psi_m - \Psi_r. \quad (4)$$

In data analysis, this resolution can be estimated through the sub-event method, see equations 14 and 15 in [25]. However, in a simulated environment, Ψ_r is known and can be artificially smeared to Ψ_m by a given resolution through the following probability density function,

$$\frac{dP}{d(\Delta\Psi_m)} = \frac{1}{2\pi} \left[\exp\left(-\frac{\chi_m^2}{2}\right) + \sqrt{\frac{\pi}{2}}\chi_m \cos(m\Delta\Psi_m) \right. \\ \left. \times \exp\left(-\frac{\chi_m^2 \sin^2(m\Delta\Psi_m)}{2}\right) \right. \\ \left. \times \left(1 + \text{erf}\left(\frac{\chi_m \cos(m\Delta\Psi_m)}{\sqrt{2}}\right)\right) \right]. \quad (5)$$

Where χ_m has the following relation to the event plane resolution,

$$R_m = \sqrt{\frac{\pi}{8}}\chi_m \exp\left(-\frac{\chi_m^2}{4}\right) \left[I_0\left(\frac{\chi_m^2}{4}\right) + I_1\left(\frac{\chi_m^2}{4}\right) \right]. \quad (6)$$

I_0 and I_1 are modified Bessel functions of the first kind [26].

When analyzing real data in the global frame, Ψ_m can be used to estimate the direction of \hat{b} ; therefore, the daughter kaon angles θ^* and β are also estimations, leading to a shift in the observed SDMEs. The spin density matrix from the event plane, ρ^{Ψ_m} , can be related to the spin density matrix from the reaction plane, ρ , by considering a spin-1 space rotation of ρ around the global frame $+x$ -axis. The spin-1 x-rotation operator can be written as follows,

$$\mathbf{R}_x(\Delta\Psi_m) = e^{-i\Delta\Psi_m J_x} \\ = \begin{pmatrix} \frac{1+\cos\Delta\Psi_m}{2} & \frac{-i\sin\Delta\Psi_m}{\sqrt{2}} & \frac{-1+\cos\Delta\Psi_m}{2} \\ \frac{-i\sin\Delta\Psi_m}{\sqrt{2}} & \cos\Delta\Psi_m & \frac{-i\sin\Delta\Psi_m}{\sqrt{2}} \\ \frac{-1+\cos\Delta\Psi_m}{2} & \frac{-i\sin\Delta\Psi_m}{\sqrt{2}} & \frac{1+\cos\Delta\Psi_m}{2} \end{pmatrix} \quad (7)$$

where J_x is the total x-angular momentum operator in the spin-1 basis. The rotation operator is applied to ρ :

$$\rho^{\Psi_m} = \mathbf{R}_x(\Delta\Psi_m) \rho \mathbf{R}_x(\Delta\Psi_m)^\dagger. \quad (8)$$

Using the resulting matrix from Eq. (8), the parameters in Eq. (1) are calculated in the event plane frame in

terms of the reaction plane frame parameters and $\Delta\Psi_m$. The relations are as follows:

$$\begin{aligned}\rho_{00}^{\Psi_m} = & \rho_{00} \frac{1 + \cos 2\Delta\Psi_m}{2} \\ & + (1 - \rho_{00} + 2\text{Re}(\rho_{1-1})) \frac{1 - \cos 2\Delta\Psi_m}{4} \\ & + \frac{\sqrt{2}}{2} \text{Im}(\rho_{10} - \rho_{0-1}) \sin 2\Delta\Psi_m,\end{aligned}\quad (9)$$

$$\begin{aligned}\text{Re}(\rho_{10}^{\Psi_m} - \rho_{0-1}^{\Psi_m}) = & \text{Re}(\rho_{10} - \rho_{0-1}) \cos \Delta\Psi_m \\ & - \sqrt{2} \text{Im}(\rho_{1-1}) \sin \Delta\Psi_m,\end{aligned}\quad (10)$$

$$\begin{aligned}\text{Im}(\rho_{10}^{\Psi_m} - \rho_{0-1}^{\Psi_m}) = & \text{Im}(\rho_{10} - \rho_{0-1}) \cos 2\Delta\Psi_m \\ & - \frac{1}{2\sqrt{2}} [3\rho_{00} - 1 - 2\text{Re}(\rho_{1-1})] \sin 2\Delta\Psi_m,\end{aligned}\quad (11)$$

$$\begin{aligned}\text{Re}(\rho_{1-1}^{\Psi_m}) = & \frac{1}{8} [3\rho_{00} - 1 + 6\text{Re}(\rho_{1-1}) \\ & - (3\rho_{00} - 1 - 2\text{Re}(\rho_{1-1})) \cos 2\Delta\Psi_m] \\ & - \frac{1}{2\sqrt{2}} \text{Im}(\rho_{10} - \rho_{0-1}) \sin 2\Delta\Psi_m,\end{aligned}\quad (12)$$

$$\begin{aligned}\text{Im}(\rho_{1-1}^{\Psi_m}) = & \text{Im}(\rho_{1-1}) \cos \Delta\Psi_m \\ & + \frac{1}{\sqrt{2}} \text{Re}(\rho_{10} - \rho_{0-1}) \sin \Delta\Psi_m.\end{aligned}\quad (13)$$

When measuring these quantities in data, the average of each term over many events is extracted. Keeping in mind that the parameters in ρ are independent of the event plane smearing terms involving $\Delta\Psi_m$, the average over many events is taken and the reaction plane frame parameters in terms of event plane frame parameters and the averages of the cosine terms are solved. The averages of the sine terms are 0 since this is an average of an odd function over the even distribution in Eq. (5). Ignoring the average brackets for the SDMEs, the following relations are derived:

$$\begin{aligned}\rho_{00} = & \frac{1}{4\langle \cos 2\Delta\Psi_m \rangle} \left[(3 + \langle \cos 2\Delta\Psi_m \rangle) \rho_{00}^{\Psi_m} \right. \\ & \left. (-1 + \langle \cos 2\Delta\Psi_m \rangle) (1 + 2\text{Re}(\rho_{1-1}^{\Psi_m})) \right],\end{aligned}\quad (14)$$

$$\text{Re}(\rho_{10} - \rho_{0-1}) = \frac{\text{Re}(\rho_{10}^{\Psi_m} - \rho_{0-1}^{\Psi_m})}{\langle \cos \Delta\Psi_m \rangle},\quad (15)$$

$$\text{Im}(\rho_{10} - \rho_{0-1}) = \frac{\text{Im}(\rho_{10}^{\Psi_m} - \rho_{0-1}^{\Psi_m})}{\langle \cos 2\Delta\Psi_m \rangle},\quad (16)$$

$$\begin{aligned}\text{Re}(\rho_{1-1}) = & \frac{1}{8} \left[\frac{1 + 2\text{Re}(\rho_{1-1}^{\Psi_m}) - 3\rho_{00}^{\Psi_m}}{\langle \cos 2\Delta\Psi_m \rangle} \right. \\ & \left. + (-1 + 6\text{Re}(\rho_{1-1}^{\Psi_m}) + 3\rho_{00}^{\Psi_m}) \right]\end{aligned}\quad (17)$$

$$\text{Im}(\rho_{1-1}) = \frac{\text{Im}(\rho_{1-1}^{\Psi_m})}{\langle \cos \Delta\Psi_m \rangle}.\quad (18)$$

A notable feature of these relations is the dependence of ρ_{00} and $\text{Re}(\rho_{1-1})$ on both $\rho_{00}^{\Psi_m}$ and $\text{Re}(\rho_{1-1}^{\Psi_m})$, indicating a coupling of these terms when the event plane resolution is finite. This is a potential downfall for the 1-dimensional method, where an integration over the β angle in Eq. (1) is performed, only allowing for the measurement of $\rho_{00}^{\Psi_m}$. In this case, a true $\text{Re}(\rho_{1-1})$ will lead to a signal of $\rho_{00}^{\Psi_m}$, which the 1-dimensional $\cos \theta^*$ method cannot correct for, resulting in a biased final signal of ρ_{00} . For $m = 1$, the values $\langle \cos \Delta\Psi_1 \rangle$ and $\langle \cos 2\Delta\Psi_1 \rangle$ range from 0 to 1, based on how well the true reaction plane is estimated. When $m = 2$, $\langle \cos 2\Delta\Psi_2 \rangle$ also ranges from 0 to 1, but $\langle \cos \Delta\Psi_2 \rangle = 0$, since Eq. (5) is periodic over π , but $\cos \Delta\Psi_2$ is periodic over 2π . This prohibits extraction of $\text{Re}(\rho_{10} - \rho_{0-1})$ and $\text{Im}(\rho_{1-1})$ from the second order event plane in data, as terms extracted relative to the event plane frame angle are forced to 0 by $\langle \cos \Delta\Psi_2 \rangle$.

III. SIMULATION STUDIES

To test the event plane correction formalism in Eqs. (14–18), a Monte Carlo (MC) simulation sample of the decay, $\phi \rightarrow K^+ + K^-$, was created with 500M events. The results of this simulation would be qualitatively similar to other two-body decays of vector mesons into pseudo-scalar mesons, such as $K^* \rightarrow K^\pm \pi^\mp$ and $\rho \rightarrow \pi^+ \pi^-$. The model used inputs from Pythia8 simulations or published data for 20-60% centrality Au+Au collisions. The ϕ -meson p_T distribution was weighted by a Levy fit to the transverse momentum (p_T) spectrum from [27]. Pythia8 p+p collisions were sampled to estimate the rapidity (y) spectrum for ϕ -mesons [28]. The ϕ -mesons were simulated with $1.2 < p_T < 4.2$ GeV/c and $|y| < 1$, to match the kinematic selections used by the STAR Collaboration in [1]. The reaction plane angle followed a randomly generated uniform distribution. The input elliptic flow (v_2), which describes the particle emission relative to the reaction plane, was derived from fitting equation 2 from [29] to the p_T dependent v_2 data in [30]. By construction, the daughter K^+ and K^- distributions in the ϕ -meson rest frame were isotropic, which translates to $\rho_{00} = 1/3$ and $\text{Re}(\rho_{10} - \rho_{0-1}) = \text{Im}(\rho_{10} - \rho_{0-1}) = \text{Re}(\rho_{1-1}) = \text{Im}(\rho_{1-1}) = 0$. When simulating any deviation of these parameters, Eq. (1) was used to weight the 2-dimensional $\cos \theta^*, \beta$ distribution.

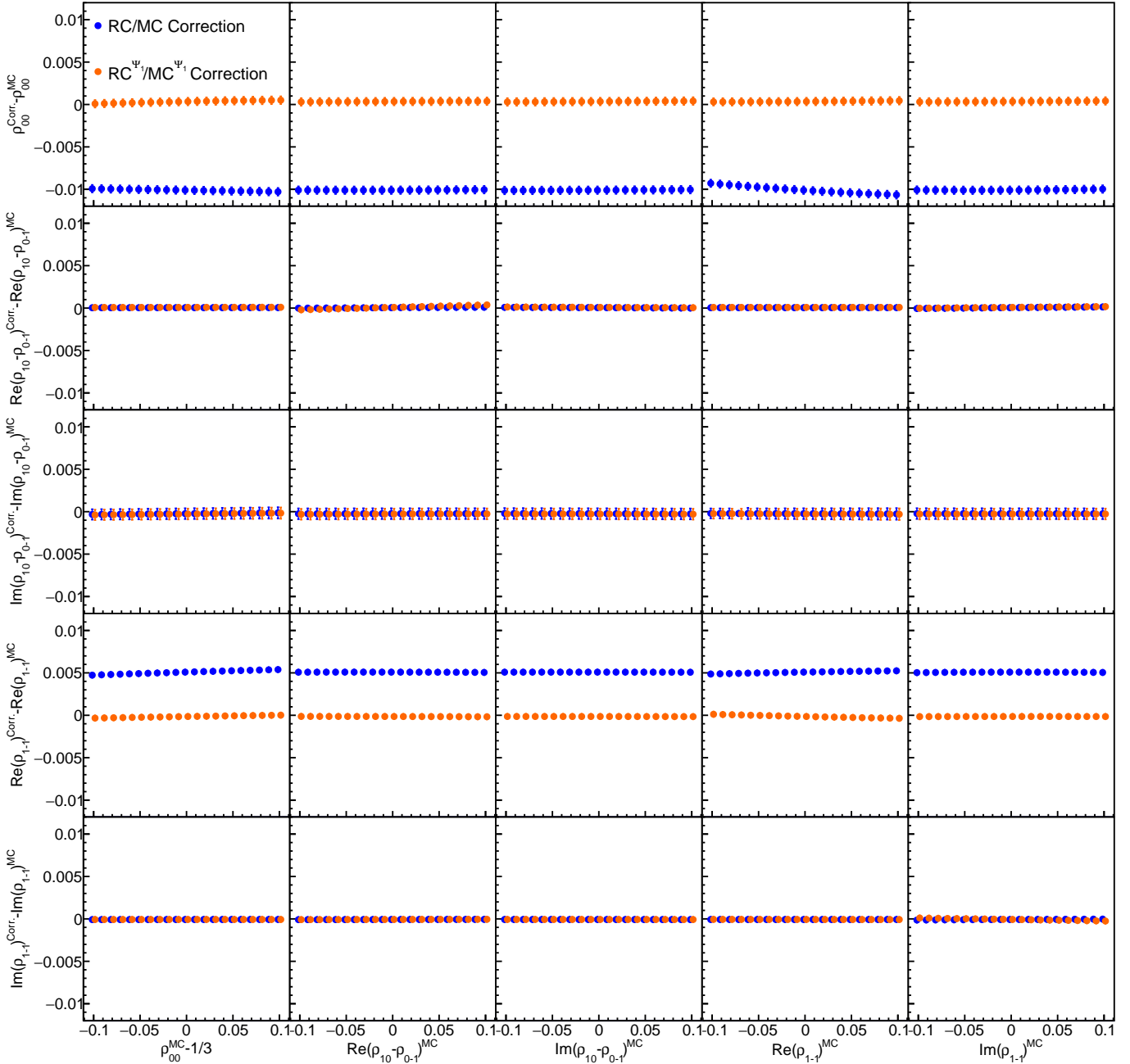


FIG. 2. 2-dimensional event plane resolution corrected results with and without event plane smearing: Blue points correspond to using the reaction plane yield correction and the orange points correspond to the event plane yield correction.

With this MC model setup, the ability to extract ρ parameters was tested when event plane smearing is present, following directly from the relations in Eqs. (14–18). Also examined were the effects of including or excluding event plane smearing in simulation when building a $\cos\theta^*,\beta$ yield correction matrix. This study started with the MC generator-level information, listed at the beginning of this section, and then variable reweighting of the $\cos\theta^*,\beta$ distributions was applied to simulate the ρ parameters. The event plane angles were smeared relative to the reaction plane angle following Eqs. (5–6),

where $R_1 = 0.6$ to roughly match the event plane resolution in STAR. The following acceptance cuts were applied on the daughter kaons: $|\eta| < 1$, $p_T > 0.1$ GeV/c, and $|\mathbf{p}| < 10$ GeV/c. Various detector efficiencies from the STAR experiment were also applied to the daughter kaons leaving reconstructed kaon tracks. The reconstructed ϕ -mesons distributions were then filled according to the K^+ momentum angles in the ϕ -meson rest frame relative to the event plane, $\cos\theta^{*\Psi_m}$ and β^{Ψ_m} , labeled RC^{Ψ_m} . In the case where there was no smearing of the event plane for the reconstructed ϕ -mesons,

the reconstructed $\cos\theta^*, \beta$ distributions are labeled RC. Similarly, the MC level $\cos\theta^*, \beta$ and $\cos\theta^{*\Psi_m}, \beta^{\Psi_m}$ distributions are labeled MC and MC^{Ψ_m} , respectively. In the isotropic case, which is used to extract the ϕ -meson yield corrections, the labels are changed to RC_0 , $\text{RC}_0^{\Psi_m}$, MC_0 , and $\text{MC}_0^{\Psi_m}$. For all of these distributions 10 equal sized bins for $\cos\theta^*$ from -1 to 1, and 10 equal sized bins for β from 0 to 2π were used. These bin sizes were chosen to mimic realistic binning for experimental heavy-ion collision data.

The distribution RC^{Ψ_m} was corrected for various ρ parameter inputs by dividing each distribution by the overall efficiency of ϕ -meson reconstruction in the isotropic case. The correction procedure was tested with the event plane smeared efficiency, $\text{RC}_0^{\Psi_m}/\text{MC}_0^{\Psi_m}$, and the reaction plane level efficiency, RC_0/MC_0 . Note that the isotropic case was used since the true ρ values in data are not known and the corrections are assumed to be independent of the input ρ . In the previous 1-dimensional method, event plane smearing was ignored in the correction procedure, and any difference between final corrected ρ parameters and the MC level parameters due to this missing feature is quantified here. To quantify any difference between final corrected ρ parameters and the MC level parameters due to ignoring the smearing of the event plane, the efficiency yield corrections are applied by dividing RC^{Ψ_m} by $\text{RC}_0^{\Psi_m}/\text{MC}_0^{\Psi_m}$ and RC_0/MC_0 , separately. Then, the event plane frame parameters ρ^{Ψ_m} were extracted from the corrected $\cos\theta^{*\Psi_m}, \beta^{\Psi_m}$ distribution by fitting with the following function:

$$\begin{aligned} \frac{d^2N}{d\cos\theta^{*\Psi_m}d\beta^{\Psi_m}} &= N_0 \left[1 - \rho_{00}^{\Psi_m} \right. \\ &+ \left(3\rho_{00}^{\Psi_m} - 1 \right) \cos^2\theta^{*\Psi_m} \\ &- \sqrt{2}\text{Re} \left(\rho_{10}^{\Psi_m} - \rho_{0-1}^{\Psi_m} \right) \sin 2\theta^{*\Psi_m} \cos\beta^{\Psi_m} \\ &+ \sqrt{2}\text{Im} \left(\rho_{10}^{\Psi_m} - \rho_{0-1}^{\Psi_m} \right) \sin 2\theta^{*\Psi_m} \sin\beta^{\Psi_m} \\ &- 2\text{Re} \left(\rho_{1-1}^{\Psi_m} \right) \sin^2\theta^{*\Psi_m} \cos 2\beta^{\Psi_m} \\ &\left. + 2\text{Im} \left(\rho_{1-1}^{\Psi_m} \right) \sin^2\theta^{*\Psi_m} \sin 2\beta^{\Psi_m} \right], \end{aligned} \quad (19)$$

where N_0 is a free normalization parameter. The final ρ parameters are calculated using Eqs. (14–18). In an actual experiment such as STAR, the distribution RC^{Ψ_m} would be replaced by the ϕ -meson yields extracted in each $\cos\theta^{*\Psi_m}$ and β^{Ψ_m} bin combination. See Extended Data Figures 1a and 1b in [1] for examples of vector meson yield extraction from STAR data.

The same procedure was repeated for the 1-dimensional method, where all distributions were integrated over the β dimensions before any corrections were derived or applied. The 1-dimensional $\rho_{00}^{\Psi_m}$ was extracted by fitting the corrected ϕ -meson yields with Eq. (19) in-

tegrated over β^{Ψ_m} :

$$\frac{dN}{d\cos\theta^{*\Psi_m}} = N_0 \left[1 - \rho_{00}^{\Psi_m} + \left(3\rho_{00}^{\Psi_m} - 1 \right) \cos^2\theta^{*\Psi_m} \right], \quad (20)$$

The reaction plane frame ρ_{00} was then calculated following Eq. (15) derived in Ref. [19], rewritten here:

$$\rho_{00} = \frac{4}{1 + 3\langle \cos 2\Delta\Psi_m \rangle} \left(\rho_{00}^{\Psi_m} - \frac{1}{3} \right) + \frac{1}{3}. \quad (21)$$

This equation can also be derived from Eq. (14) by setting all off-diagonal elements to zero, averaging over all events, and then solving for ρ_{00} .

In Figure 2, it is shown that ignoring the smearing of the event plane in the correction procedure can lead to systematic shifts in the values of the SDME parameters. This figure also shows the ability to correct for the event plane resolution for all SDME parameters regardless of which truth level parameter was varied, confirming the validity of Eqs. (14–18). Figure 3 shows the comparison of ρ_{00} extraction with the 1-dimensional and 2-dimensional extraction methods with variable input ρ_{00} and $\text{Re}(\rho_{1-1})$. The 1-dimensional ρ_{00} was corrected for event plane resolution using Eq. (21). It was found that when the true ρ_{00} is varied, both methods could recover the true value within 1%, with the 2-dimensional method having larger uncertainty and slightly better agreement with the true value. When the true $\text{Re}(\rho_{1-1})$ is non-zero, the 2-dimensional correction method can extract the true ρ_{00} value, but the 1-dimensional method cannot, as expected from (14).

Another important consideration when extracting vector meson SDMEs from particle detector data is p_T resolution. Since a detector must have some finite precision in particle tracking, it is important to understand how this affects the measured results. When measuring distributions relative to $\cos(\theta^*)$ and β , these angular quantities are directly related to the momenta of the daughter kaons and the ϕ -meson, and are therefore affected by a finite p_T resolution in a non-trivial manner.

Starting with the MC sample described at the beginning of this section, a Gaussian smearing of kaon p_T based on a 10% p_T resolution was applied. This value was chosen to emphasize the effect of the p_T resolution, and most heavy-ion collisions detectors have p_T resolutions on the order of 2–3% percent or smaller. To study this effect exclusively, no cuts or event plane smearing were applied, and the final p_T smeared distribution $\cos\theta^{*\prime}, \beta'$ was corrected using the isotropic ρ parameter case. If the p_T values in the correction procedure are not smeared, this is the same as simply extracting the ρ parameters directly from the $\cos\theta^{*\prime}, \beta'$ distributions. It is observed that ignoring the p_T resolution in correction can have a significant effect, given by the blue circles in Figure 4. The correction was also tested by taking the ratio of the p_T smeared isotropic $\cos\theta^{*\prime}, \beta'$ distribution over the non-smeared distribution, and then dividing the $\cos\theta^{*\prime}, \beta'$ distribution with various input ρ parameters by this ratio.

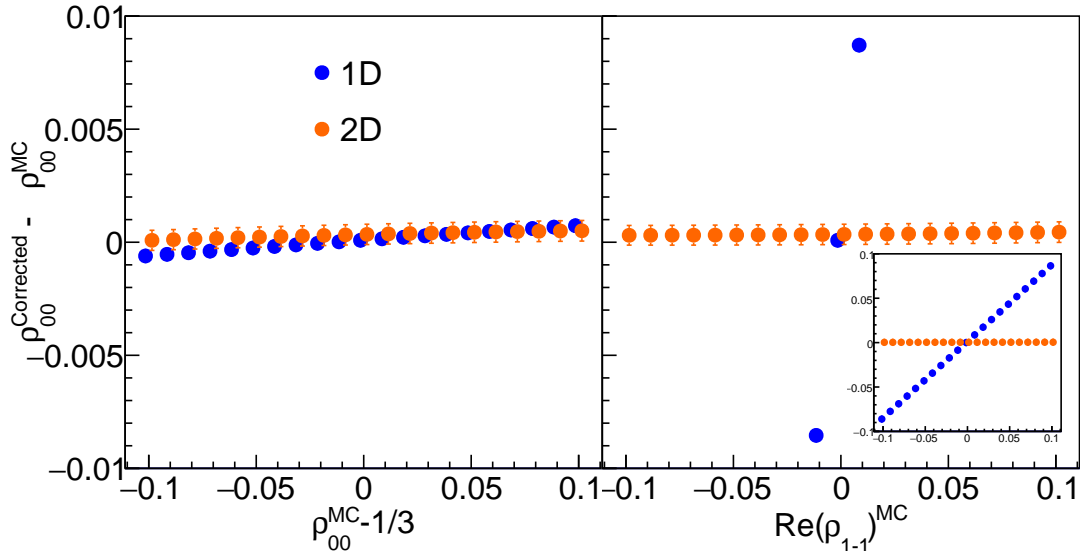


FIG. 3. 1-dimensional and 2-dimensional event plane resolution correction: Blue points correspond to using the 1-dimensional method and orange points correspond to the 2-dimensional method.

Ideally, this would correct for the p_T smearing and the MC level input parameters would be retrieved; however, as seen in Figure 4, a difference is observed between the corrected ρ values in the 0th iteration and the input MC values, displayed as yellow squares. At p_T resolutions of 2-3%, the deviations of corrected SDME values from MC are roughly 10-20% of what is observed for 10% p_T resolution.

To address the ρ parameter dependence of the p_T resolution effect, the corrections can be recalculated using the output ρ parameters from the previous iteration. This iterative method was tested in Figure 4 and it is shown that after just one iteration the input MC ρ values are recovered. Therefore, when analyzers are measuring ρ parameters, iterating the correction procedure at least one time should provide a more accurate measurement of the true value.

IV. CONCLUSION

The measurement of vector meson global SDMEs in heavy-ion collisions requires careful consideration of various factors, some of which were studied in this paper. Event plane resolution correction formulas were derived for all five global SDME parameters and were validated using a Monte Carlo simulation study with realistic efficiency and acceptance effects. In deriving these corrections, it was discovered that for even order harmonic event planes, it is not possible to extract $\text{Re}(\rho_{10} - \rho_{0-1})$

and $\text{Im}(\rho_{1-1})$ as these quantities are forced to zero. Through Monte Carlo studies, it was found that event plane smearing is required in the correction procedure, and without it there is a systematic shift of the extracted SDME parameters. Additionally, it was shown that when event plane smearing is present, a 1-dimensional extraction of ρ_{00} from the $\cos \theta^*$ distribution of ϕ -mesons with a non-zero $\text{Re}(\rho_{1-1})$ will bias the output ρ_{00} value. This emphasizes the importance of performing a 2-dimensional extraction of all SDME parameters. The p_T resolution was also considered, where it was discovered that the effect from this resolution depends on the true SDME values. By recalculating the particle yield corrections with SDME values from the previous iteration the results converge with the true input values within three iterations. The methods discussed in this paper are crucial for proper measurements of vector meson global SDME parameters.

ACKNOWLEDGMENTS

Thank you to A.-H. Tang and D. Shen for many fruitful discussions. Gavin Wilks is partially supported by the U.S. Department of Energy under Contract No. DE-FG02-94ER40865. Zhenyu Ye is partially supported by the U.S. Department of Energy under Contract No. DE-AC02-05CH11231. Xu Sun is partially supported by National Natural Science Foundation of China (NSFC) under Grant No. 12475147.

[1] M. S. Abdallah *et al.* (STAR Collaboration), Pattern of global spin alignment of ϕ and K^{*0} mesons in heavy-ion

collisions, *Nature* **614**, 244 (2023).

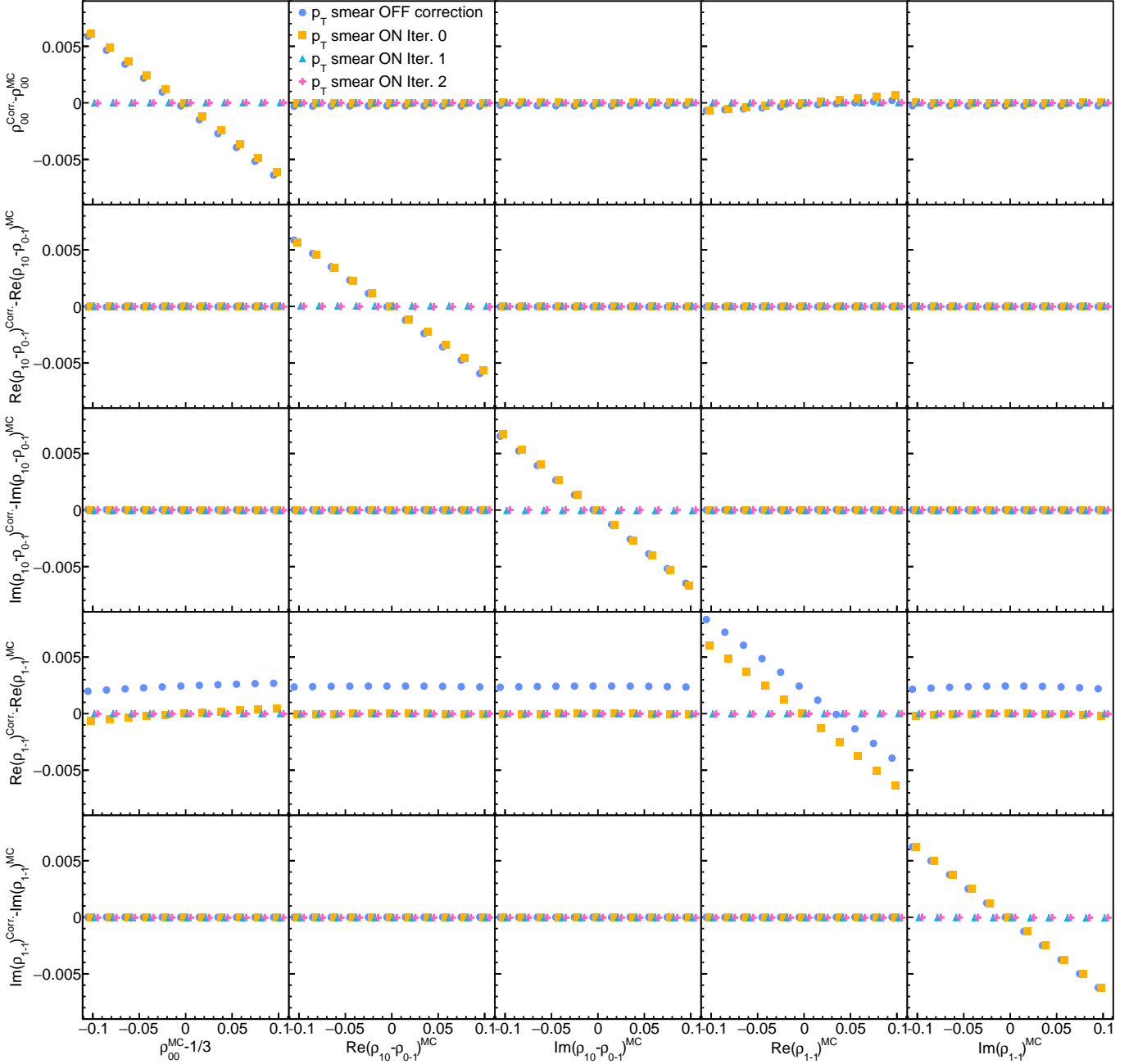


FIG. 4. p_T resolution correction with iterative method: The blue circles correspond to p_T smearing off in the correction procedure. Yellow squares correspond to the first attempt (iteration 0) at correcting the p_T resolution effect using isotropic $\cos \theta^*, \beta$ MC. The cyan triangles and pink crosses correspond to the first and second iteration of input MC ρ parameters, respectively.

- [2] J.-H. Chen *et al.*, Properties of the QCD matter: review of selected results from the relativistic heavy ion collider beam energy scan (RHIC BES) program, *Nucl. Sci. Tech.* **35**, 214 (2024).
- [3] Z.-T. Liang and X.-N. Wang, Spin alignment of vector mesons in non-cnetral a+a collisions, *Phys. Lett. B* **629**, 20 (2005).
- [4] Y.-G. Yang, R.-H. Fang, Q. Wang, and X.-N. Wang, Quark coalescence model for polarized vector mesons and baryons, *Phys. Rev. C* **97**, 034917 (2018).
- [5] J.-H. Gao, Helicity polarization in relativistic heavy ion collisions, *Phys. Rev. D* **104**, 076016 (2021).
- [6] B. Müller and D.-L. Yang, Anomalous spin polarization from turbulent color fields, *Phys. Rev. D* **105**, L011901 (2022).
- [7] X.-L. Xia, H. Li, X.-G. Huang, and H.-Z. Huang, Local spin alignment of vector mesons in relativistic heavy-ion collisions, *Phys. Lett. B* **817**, 136325 (2021).
- [8] e. a. L. Adamczyk (STAR Collaboration), Global λ hyperon polarization in nuclear collisions, *nature* **548**,

62–65 (2017).

[9] e. a. J. Adam (STAR Collaboration), Global polarization of Λ hyperons in $\text{au} + \text{au}$ collisions at $\sqrt{s_{NN}} = 200$ gev, Phys. Rev. C **98**, 014910 (2018).

[10] e. a. M. S. Abdallah (STAR Collaboration), Global Λ -hyperon polarization in $\text{Au} + \text{Au}$ collisions at $\sqrt{s_{NN}} = 3\text{GeV}$, Phys. Rev. C **104**, L061901 (2021).

[11] e. a. M. I. Abdulhamid (STAR Collaboration), Global polarization of Λ and $\bar{\Lambda}$ hyperons in $\text{Au} + \text{Au}$ collisions at $\sqrt{s_{NN}} = 19.6$ and 27 gev, Phys. Rev. C **108**, 014910 (2023).

[12] X.-L. Sheng, L. Oliva, and Q. Wang, What can we learn from the global spin alignment of ϕ mesons in heavy-ion collisions?, Phys. Rev. D **101**, 096005 (2020).

[13] X.-L. Sheng, L. Oliva, and Q. Wang, Erratum: What can we learn from the global spin alignment of ϕ mesons in heavy-ion collisions?, Phys. Rev. D **105**, 099903 (2022).

[14] X.-L. Sheng, L. Oliva, and X.-N. Wang, Improved quark coalescence model for spin alignment and polarization of hadrons, Phys. Rev. D **102**, 056013 (2020).

[15] X.-L. Sheng, L. Oliva, Z.-T. Liang, Q. Wang, and X.-N. Wang, Phys. Rev. Lett. **131**, 042304 (2023).

[16] X.-L. Sheng, S. Pu, and Q. Wang, Momentum dependence of the spin alignment of the ϕ meson, Phys. Rev. C **108**, 054902 (2023).

[17] Y.-Q. Z. Xin-Li Sheng, S.-W. Li, F. Becattini, and D. Hou, Holographic spin alignment for vector mesons, Phys. Rev. D **110**, 056047 (2024).

[18] J.-p. Lv, Z.-h. Yu, Z.-t. Liang, Q. Wang, and X.-N. Wang, Global quark spin correlations in relativistic heavy ion collisions, Phys. Rev. D **109**, 114003 (2024).

[19] A. H. Tang, B. Tu, and C. S. Zhou, Practical considerations for measuring global spin alignment of vector mesons in relativistic heavy ion collisions, Phys. Rev. C **98**, 044097 (2018).

[20] Z. Wang, J. Chen, D. Shen, A. Tang, and G. Wang, Effect of vector meson spin coherence on the observables for the chiral magnetic effect in heavy-ion collisions, Phys. Rev. C **111**, 014910 (2025).

[21] K. J. Gonçalves and G. Torrieri, Spin alignment of vector mesons as a probe of spin hydrodynamics and freeze-out, Phys. Rev. C **105**, 034913 (2022).

[22] P. H. D. Moura, K. J. Gonçalves, and G. Torrieri, Quarkonium spin alignment in a vortical medium, Phys. Rev. D **108**, 034032 (2023).

[23] K. J. Gonçalves, G. Torrieri, and R. Ryblewski, Meson spin alignment and baryon polarization from coalescence with spin-vorticity nonequilibrium, Phys. Rev. C **112**, 014901 (2025).

[24] K. Schilling, P. Seyboth, and G. E. Wolf, On the analysis of vector-meson production by polarized photons, Phys. B **15**, 397 (1970).

[25] A. M. Poskanzer and S. A. Voloshin, Methods for analyzing anisotropic flow in relativistic nuclear collisions, Phys. Rev. C **58**, 3 (1998).

[26] S. Voloshin and Y. Zhang, Flow study in relativistic nuclear collisions by Fourier expansion of azimuthal particle distributions, Z. Phys. C **70**, 665 (1996).

[27] L. Adamczyk *et al.* (STAR Collaboration), Probing parton dynamics of QCD matter with Ω and ϕ production, Phys. Rev. C **93**, 021903(R) (2016).

[28] T. Sjöstrand *et al.*, An introduction to PYTHIA 8.2, Comput. Phys. Commun. **191**, 159 (2015).

[29] X. Dong, S. Esumi, P. Sorensen, N. Xu, and Z. Xu, Resonance decay effects on anisotropy parameters, Phys. Lett. **597**, 328 (2004).

[30] L.-K. Liu, Elliptic and triangular flow of (multi-)strange hadrons and ϕ mesons in BES-II energies at STAR, EPJ Web of Conferences **276**, 01018 (2023).

[31] B. I. Abelev *et al.* (STAR Collaboration), Partonic flow and ϕ -meson production in $\text{au} + \text{au}$ collisions at $\sqrt{s_{NN}}$ GeV, Phys. Rev. C **79**, 064903 (2007).